0 0 0 0 4 2 0 7 8 7 8

Submitted to Metallurgical Transactions

LBL-3559
Preprint c.1

# HIGH RESOLUTION STUDY OF ORDERING REACTIONS IN GOLD-CHROMIUM ALLOYS

RECEIVED
LAWRENCE
BERKELEY LABORATORY
SEP 17 1975
LIBRARY AND
DOCUMENTS SECTION

J. Dutkiewicz and G. Thomas

February 1975

Prepared for the U. S. Energy Research and
Development Administration under Contract W-7405-ENG-48

For Reference

Not to be taken from this room

LAWRENCE BERKELEY LABORATORY
UNIVERSITY OF CALIFORNIA
BERKELEY

LBL-3559
c.1

## DISCLAIMER

This document was prepared as an account of work sponsored by the United States Government. While this document is believed to contain correct information, neither the United States Government nor any agency thereof, nor the Regents of the University of California, nor any of their employees, makes any warranty, express or implied, or assumes any legal responsibility for the accuracy, completeness, or usefulness of any information, apparatus, product, or process disclosed, or represents that its use would not infringe privately owned rights. Reference herein to any specific commercial product, process, or service by its trade name, trademark, manufacturer, or otherwise, does not necessarily constitute or imply its endorsement, recommendation, or favoring by the United States Government or any agency thereof, or the Regents of the University of California. The views and opinions of authors expressed herein do not necessarily state or reflect those of the United States Government or any agency thereof or the Regents of the University of California.

0 0 0 0 4 2 0 7 8 7 9



# HIGH RESOLUTION STUDY OF ORDERING REACTIONS IN GOLD-CHROMIUM ALLOYS

J. Dutkiewicz* and G. Thomas

Department of Materials Science and Engineering, and Lawrence Berkeley Laboratory, University of California, Berkeley, California, 14720

## ABSTRACT

The ordering reactions in $Au_4Cr$ and $Au_3Cr$ alloys have been investigated using high resolution dark field and lattice imaging techniques. In all cases the ordered structures can be described in terms of compositional modulations as occur during spinodal decomposition. In alloys quenched from above the critical temperature s.r.o. microdomains of size 10-15Å have been resolved with structures resresented by modulations in composition along <420>. After aging the $Au_4Cr$ alloy below $T_c$ the Dla lro phase appears as ordered domains of size 50-100Å showing composition modulations with wavelength of 5d<531>. These domains grow in size up to 500Å becoming finally the Dla fully ordered structure.

A new observation has been made in the $Au_3Cr$ alloy, viz that the lro structure is non-stoichiometric $L1_o$ with $\lambda_{[001]}$ = 4Å. The transformation from sro in this alloy occurs with the formation of a transitional ordered phase, (similar to $DO_{22}$), which can be described in terms of composition modulations along [001], with wavelength equal to the c parameter (8Å) of the $DO_{22}$ structure.

Lattice imaging of the two variants of superlattice planes in ordered $Au_4Cr$ enabled the atomic arrangement in the area of translational and rotational antiphase boundaries to be determined.

---

*On one year leave from the Institute of Metallurgy, Polish Academy of Sciences, 30-059 Krakow, ul. Reymonta 25, Poland.

## INTRODUCTION

Gold-chromium alloys show a wide range of solid solubility of chromium in gold, viz. up to 43 at %Cr at 1150°C. Disordered fcc alloys near the composition $Au_4Cr$ form the ordered D1a structure on ordering below the critical temperature ~330°C. As can be seen in Fig. 1a, the D1a structure has tetragonal symmetry with chromium atoms occupying every fifth {420} and {620} plane of the original fcc solid solution. Among other structures, which may appear in this system are the tetragonal $DO_{22}$ and $L1_o$ superlattices, which are schematically shown in Fig. 1b and 1c (see refs 1,3).

Alloys containing up to 25 at %Cr show the existence of short range order at temperatures close to and above $T_c$. The nature of sro in these alloys is similar to that existing in $Ni_4Mo$ and $Au_4V$ and has been the subject of a number of investigations.[1-4] Alloys quenched from temperatures above $T_c$ show diffuse $\{1\frac{1}{2}0\}$ superlattice maxima in the diffraction pattern, which are probably caused by the presence of imperfectly ordered $DO_{22}$ and D1a microdomains.[3] Okamoto and Thomas[2] proposed a model of sro based on composition modulations along the <210> directions analogous to the spinodal approach to order disorder transformation due to Cook and de Fontaine.[5] The presence of sinusoidal composition modulations of wavelength close to $4(d_{420})$ explains the absence of {110} and {210} superlattice spots and the elongated shape of the superlattice maxima by the presence of weak satellites near the superlattice positions. The diffuse scattering maxima corresponding to sro are observed at different reciprocal lattice positions to those of the long range ordered phase existing below $T_c$. The mechanism of the transforma-

tion from short to long range order (which has the Dla structure) has not been studied in detail, although it may have significant influence on the final domain structure.

The ordering transformations occur on a very fine atomic scale, and as shown by dark field electron microscopy studies using the $\{1\frac{1}{2}0\}$ reflections in the $Ni_4Mo$ alloy[3] the size of the domains, visible as light contrast regions, is in the range 20-40Å in diameter. These images may not, however, be representative of the actual size and distribution of the microdomains according to Cowley's theoretical calculations, based on the phase object approximation.[6] The intensity of the superlattice dark field image is often very low and therefore the dark field micrograph is affected by the electron noise background. This difficulty can be eliminated using the lattice imaging technique, and it has been recently applied to the study of ordering in $Cu_3Au$[7] and niobium-tungsten oxides.[8] The interpretation of lattice images of ordered alloys based on the dynamical theory of electron diffraction has been given in the recent paper by Sinclair et al.[7] It was shown that the contrast of lattice images depends on the crystal orientation, foil thickness, defocus of the objective lens, degree of order and the position of the domain in the foil. The optimum conditions of fringe visibility were found to be at a foil thickness of 250-300Å, with objective lens defocus in the range 0-300Å, depending on the illumination tilt and aperture position. For lattice images taken with tilted illumination in which the superlattice reflection g coincides with the optic axis of the microscope, and the 0,g,2g beams are included in the objective aperture, the optimum fringe contrast occurs at objective

defocus equal to 300Å. Using this mode of imaging the small domains existing in partially ordered $Cu_3Au$ alloy were revealed as regions of double fringe periodicity existing in the disordered matrix represented by the fcc {200} fringes.[7] The application of this technique is however, more difficult in the case of gold-chromium alloys, because there is no fundamental spacing ≥2Å in any superlattice row of the Dla structure. Therefore, only the superlattice $\{1\frac{1}{2}0\}$ or $\{\frac{4}{5},\frac{2}{5}0\}$ planes can be resolved. Calculations have been performed of the contrast for lattice images as a function of thickness, defocus, orientation and degree of order in $Au_4Cr$ and other systems. The details of these will be published elsewhere;[9] the results are compatible with the calculations for $Cu_3Au$.[7]

Recent studies of domain interfaces in $Ni_4Mo$ alloys,[10] which have the identical Dla lro structure to that of $Au_4Cr$, have shown a large variety of twin, rotational, and dissociated antiphase domain boundaries (APB). Similar to results obtained by lattice imaging of ceramic materials,[8,11] lattice images taken of ordered alloys in symmetrical orientations are also very useful in the study of domain interfaces. Consequently, this technique was applied in the present work to study the geometry of domain interfaces in partially and fully ordered alloys.

## 2. EXPERIMENTAL PROCEDURE

The $Au_3Cr$ and $Au_4Cr$ alloys were cast in an arc furnace under an argon atmosphere. Chemical analysis showed that the chromium content was 27.1 and 18.3 at %Cr, in $Au_3Cr$ and $Au_4Cr$ respectively. After homogenization at 800°C the ingots were rolled down to 0.3mm thickness.

The $Au_4Cr$ thin film specimens were obtained from bulk by evaporation onto a rock salt crystal at a temperature of 450°C. The thickness of the film was calculated from the amount of the material and its distance to the substrate. The heat treatment was done with the films on the salt crystals in a microfurnace contained in the evaporator. Thin foils from $Au_3Cr$ alloy were prepared from bulk using jet electropolishing at 30°C at 18 volts in cyanide solution. This was necessary because evaporation techniques failed to yield the $Au_3Cr$ composition (see section 3).

The chemical composition of the evaporated films was checked by x-ray diffraction studies of the lattice parameter. The data were obtained using a Picker diffractometer with LiF monochromator and CuKα radiation.

The Philips 301 and Siemens 102 electron microscopes operating at 100 and 125 kV respectively were used for the high resolution study. Lattice images were chosen from a through focus series taken in a 900Å range of objective lens focal length settings.

## 3. RESULTS

In the evaporated $Au_3Cr$ alloy the Dla lro superlattice is formed as has also been found in previous research.[1,3] This superlattice structure corresponds to the $A_4B$ stoichiometric composition. This phenomenon may be due to nonstoichiometric ordering in local regions, but may also be caused by a change of composition during the evaporation process. The composition of the evaporated films was checked using x-ray diffraction measurements of the disordered fcc unit cell lattice

parameter ($a_o$). Figure 2 shows the relationship between this parameter and the chromium content determined by chemical analysis. The curve was plotted based on the x-ray measurements of $a_o$ of bulk $Au_3Cr$ and $Au_4Cr$ of exactly known composition and the lattice parameter of gold given by the ASTM standard. The measurements of the fcc $a_o$ of the evaporated film in the as-quenched state (obtained after three evaporation processes) indicate that it has the value close to that of bulk $Au_4Cr$ alloy. This means that during evaporation of the alloy of 27.1 at % chromium, chromium loss occurs such that the final composition of the evaporated film corresponds approximately to $Au_4Cr$ (20 at %Cr).

a) Evaporated $Au_4Cr$

In order to study the transformation from sro to the equilibrium D1a lro structure, a series of diffraction patterns and dark-field micrographs were taken after different aging times at 270°C. The [001] orientation of the evaporated film was convenient to study the ordering reactions because it shows the $\{1\frac{1}{2}0\}$ and $\{\frac{4}{5},\frac{2}{5},0\}$ superlattice reflections, characteristic for $DO_{22}$ and D1a structure respectively.(3) Figure 3 shows a representative set of [001] diffraction patterns and superlattice dark-field micrographs taken after 0, 16h and 70h of aging at 270°C. The [001] diffraction pattern shown in Fig. 3a was taken after quenching from 400°C. It shows the characteristic sro $\{1\frac{1}{2}0\}$ diffuse superlattice reflections. The dark-field micrograph shown in Fig. 3b was taken with the superlattice spot marked with a circle on the diffraction pattern. It shows the existence of a great number of ordered

microdomains of size 15-40Å. Since the majority of them has a size of 20Å, the appearance of larger microdomains may be caused by partial overlapping of images formed from domains along the z axis (direction of the beam.).

The diffraction pattern taken after 16h of aging at 270°C is shown in Fig. 3c. The diffraction pattern taken at slightly tilted condition (shown in the corner of Fig. 3d) shows the presence of the superlattice reflections in the <531> row. The $(1\frac{3}{5},\frac{1}{5})$ superlattice dark-filed micrograph (Fig. 3d) shows ordered microdomains of size 100-200Å.

During further aging the ordering process is completed with the formation of the lro Dla superlattice. The diffraction pattern taken after 70h of aging at 270°C (Fig. 3e) shows the higher intensity $\{\frac{4}{5},\frac{2}{5}0\}$ and $\{\frac{6}{5},\frac{2}{5}0\}$ superlattice spots, i.e. the {110} and {200} spots of the tetragonal Dla superlattice. Dark-field micrographs taken with the $(\frac{4}{5},\frac{2}{5}0)$ superlattice reflection show the existence of ordered domains of size 150-500Å. The dark-field taken with $(\frac{2}{5},\frac{4}{5}0)$ superlattice spot shows ordered domains in the areas which match those in dark contrast in Fig. 3f. This means that two variants of ordered domains exist in the specimen.

Lattice images were taken after the same aging times (as indicated in Fig. 3) at close to symmetrical orientation, in order to obtain maximum fringe contrast. 3.6Å lattice images of the $\{1\frac{1}{2}0\}$ superlattice planes taken from the $Au_4Cr$ thin film quenched from 400°C are shown in Fig. 4. As can be seen from the diffraction pattern shown in the

corner of the micrograph, it was taken at the orientation close to [001] at which two variants of the superlattice $\{1\frac{1}{2}0\}$ spots were strongly excited. The position of the objective aperture, including all the first order superlattice reflections is marked on the diffraction pattern. The micrograph was taken at a defocus of ~150Å of the objective lens which is the best condition for fringe contrast as determined from several micrographs taken in a through focus series. The contrast of fringes is relatively low, probably because of the small size of the domains (10-15Å) depending also on the local degree of order and the position of the domain in the foil.[7] In places marked by the letter A the $(\frac{1}{2}10)$ fringes of spacing 3.6Å are seen, while in the places marked by B the cross grating of fringes is observed, indicating where overlapping occurs of images of the two variants of microdomains.

Figure 5 is a high resolution micrograph taken after 16hr aging at 270°C, at a foil orientation in order to obtain two variants of the $\{\frac{1}{5},\frac{3}{5}1\}$ and $\{\frac{2}{5},\frac{4}{5}0\}$ superlattice reflections. The 3.4Å fringes visible in the micrograph correspond to the $(\bar{1}\frac{3}{5},\frac{1}{5})$ superlattice planes. In a few places in the micrograph 7.0Å fringes are seen; these correspond to the rotation moiré pattern resulting from overlapping of two variants of the ordered domains. This indicates that lro is initiated by a periodic fluctuation in composition with wavelength $\lambda = 5d\langle 351\rangle$ . The 4.5Å fringes correspond to the $(\frac{4}{5},\frac{2}{5}0)$ superlattice planes of the equilibrium Dla lro superlattice.

In the places marked by letters A and B two interesting types of domain interfaces were observed. In the region marked A, the fringe

spacing changes such that the distance between two interplanar {110} D1a spacings, indicated by arrows, is equal to $9d_{420}$ instead of $10d_{420}$. The space between them shows no fringe contrast which means that one $\{\frac{4}{5},\frac{2}{5}0\}$ plane is not occupied by the chromium atoms. Such a domain interface is energetically unstable and it may lower its energy when it dissociates into two translational APB's, or when it changes its orientation to become a translational APB. An example of the latter is marked by letter B, where the distance between the three interplanar {110} D1a spacings, marked by arrows, is equal to $13d_{420}$ instead of $15d_{420}$. As can be seen from the micrograph, such a situation may arise when two growing domains join together and the distance between them differs from a multiple of $5d_{420}$.

The lattice image shown in Fig. 6 was taken from the completely ordered alloy aged 70h at 270°C. As can be seen from the diffraction pattern shown in the corner of the micrograph, an orientation has been chosen such that $(\frac{4}{5},\frac{2}{5}0)$ and $(\frac{2}{5},\frac{4}{5}0)$ superlattice reflections (included in the objective aperture) corresponding to the two variants of the ordered domains were equally strongly excited. Rotational APB's visible in several places in the micrograph run in random directions; no twin interfaces (reported to exist in some D1a superlattice[10]) can be found in this or other similar micrographs. In a few places marked at A and B, translational antiphase boundaries are seen. They are often associated with a wedge-like curvature of the adjacent domain wall. These two types of translational APB correspond to the $\frac{1}{5}a\langle 420\rangle$ (A) or $\frac{2}{5}a\langle 420\rangle$ (B) translation of the superlattice planes. The first type of APB is visible as a line of weak contrast while in the second case is manifested as a line of no contrast. In a few places close to the

rotational APB, the cross grating of superlattice fringes can be seen. This indicates that the domain interface is inclined to the plane of the foil. Although the width of this area is only 5-10Å, it is clearly seen and demonstrates the advantage of lattice imaging over conventional dark field imaging for resolving fine scale details. Figure 7 shows the scheme illustrating the atomic arrangement in the area marked by a square in Fig. 6. The translational APB following the fcc <110> direction can be described by a displacement vector $\bar{R} = (110)a[\frac{1}{2}00]$. There is no unique crystallographic relationship in the case of rotational domain interfaces. However, it can be seen that some columns of chromium atoms may be common for two variants of superlattice planes forming rotational APB's.

b) $Au_3Cr$

Although short range order in $Au_3Cr$ has been found to be identical to that in $Au_4Cr$, the nature of lro in the former has not yet been identified.[3] Figure 8 shows a set of electron diffraction patterns and superlattice dark field micrographs taken of a foil from a bulk $Au_3Cr$ specimen after different times of aging. Figure 8a shows the [001] diffraction pattern taken after quenching from 400°C. It is very similar to the diffraction pattern obtained after quenching the $Au_4Cr$ alloy. The corresponding dark field micrograph taken with the $(1\frac{1}{2}0)$ superlattice spot (marked in the micrograph) shows small bright microdomains about 20-40Å in diameter. The area in the adjacent grain does not show any similar type of bright contrast which indicates that the electron noise effect is in this case small and the interpretation of microdomain contrast to be correct.

The diffraction pattern taken after 5 days of aging at 270°C (Fig. 8c) shows the {100} and {110} superlattice reflections which do not exist after quenching. The diffraction pattern is similar to that obtained from $Ni_3V$ [12] showing $DO_{22}$ lro, although the $\{1\frac{1}{2}0\}$ reflections in $Au_3Cr$ show much lower intensity than the {100} and {110} superlattice spots. Calculations of the structure factor for the $DO_{22}$ structure indicate that $F_{110} = F_{002} = F_{101} = 2(f_{Au} - f_{Cr})$. (The (110), (002), (101) reflections of $DO_{22}$ structure correspond to the (110), (001), $(10\frac{1}{2})$ fcc superlattice spots respectively). In $Au_3Cr$ the $\{1\frac{1}{2}0\}$ spots are significantly weaker than {100} and {110} superlattice spots, which suggests that they originate from a different type of superlattice. The corresponding dark field micrograph (Fig. 8d) taken with the $(1\frac{1}{2}0)$ spot shows the existence of microdomains of size 20-40Å which is similar to the quenched alloy. The (100) superlattice dark field micrograph (Fig. 8e) shows the existence of a few ordered domains of size close to 100Å, elongated in the <100> direction.

Figure 8f shows the [001] diffraction pattern taken from the specimen aged for 30 days at 300°C. It indicates much stronger {100} and {110} superlattice reflections, while the $\{1\frac{1}{2}0\}$ spots have become significantly weaker. It also shows the presence of very weak $\{\frac{1}{2}00\}$ reflections, which do not fit any of the superlattices known for fcc solid solutions. The {100} dark field micrograph (Fig. 8h) shows the existence of a great number of ordered domains of the size 100-200Å elongated in the <100> direction. The $\{1\frac{1}{2}0\}$ superlattice dark field micrograph (Fig. 8g) shows two types of ordered domains, a very small one of size ~20Å and larger ones (50-100Å) which appear in the same

place as the domains visible in the {100} dark field, i.e. they seem to be a part of the latter ones. The results of Fig. 8 indicate that the $1\frac{1}{2}0$ weak reflections are those remaining from the quenched-in sro state (~20Å domains). But after longer aging times (Fig. 8g) the $1\frac{1}{2}0$ dark field also reveals larger domains and since this cannot be from the $L1_o$ structure a probable explanation is due to the intermediate stage of ordering as discussed below.

The next set of micrographs (Fig. 9) was taken from a specimen aged for 30 days at 300°C in order to provide additional information about the nature of the lro. The diffraction pattern (Fig. 9a) shows the symmetrical [001] orientation. In the bright field image (Fig. 9b), the strain field contrast around the elongated domains is clearly visible. In the (010) and (100) dark field micrographs (Fig. 9c,e), domains elongated in the [100] and [010] directions are shown. By observing the bend contours it can be seen that the visibility varies from place to place and at intersecting contours the visibility of corresponding domains in Figs. 9c-e is not equal. If during ordering the $L1_2$ structure had formed (which could be assumed to happen due to the appearance of {100} and {110} superlattice reflections and the $A_3B$ stoichiometric composition) the image of the ordered domains near intersecting contours should be identical of (100), (010), and (110) dark field micrographs. The fact that this is not so (Fig. 9) supgests that the ordered phase has the $L1_o$ superlattice structure, i.e. the (100), (010) and (110) spots are from different variants. From the dark field micrographs it can also be seen that these ordered regions are disc shaped with {100} habit planes.

Figure 10 shows the lattice image taken at symmetrical orientation

from a thin foil of the $Au_3Cr$ alloy aged at 270°C for 30 days. The objective aperture was placed symmetrically to include all the first order superlattice reflections. As can be seen from this micrograph the (100) superlattice planes of spacing equal to 4Å, lying parallel to the {100} habit planes, were resolved. In some planes fringes of double periodicity, corresponding to the presence of the $(\frac{1}{2}00)$ superlattice reflections are seen (at X fig. 11). This phenomenon may be due to <100> compositional modulations corresponding to a transitional ordered phase during the transformation from the sro modulations into the $L1_0$ ordered domains. Finally, a high resolution micrograph (Fig. 11) was taken with tilted illumination, (aperture including (000) and $(\bar{2}00)$ fundamental reflections), and about 800Å defocus of the objective lens. The absence of (200) lattice fringes can be due to loss of contrast (non-ideal defocus or foil thickness). The contrast of the (100) and $(\frac{1}{2}00)$ fringes is very similar to that on the previous micrograph. The equivalence of the lattice image and the superlattice dark field (lower corner of Fig. 11) shows good agreement. Only one domain marked by "x" in the lattice image (Fig. 11) is not seen in the superlattice dark field. Since in this domain predominantly the $(\frac{1}{2}00)$ fringes are seen it is most probably the transitional ordered phase which may not appear in the (100) superlattice dark field.

## DISCUSSION OF RESULTS

### 1. SRO in Au-Cr Alloys

The recent work[3] on sro in $Au_4Cr$ and $Au_4V$ alloys explains the presence of weak scattering near various superlattice positions (predominantly at $\{1\frac{1}{2}0\}$ positions) by the existence of imperfectly

ordered $DO_{22}$ and $Dl_a$ type microdomains. This observation was confirmed in the present study by the superlattice dark field and lattice imaging results. The latter technique shows directly the superlattice periodicity and gives more reliable evidence of microdomains than conventional dark field images.[6] The occurrence of microdomains can be explained by compositional modulations[2] similar to spinodal ordering discussed by de Fontaine et al.[5] Figure 12 shows a schematic representation of the sro composition modulations along <420> . In this model,[2] the concentration wave is explained by the presence of imperfectly ordered microdomains containing nonconservative antiphase domain boundaries. The most recent work of de Fontaine[5] has shown that the nature of the concentration wave can be calculated from the K-space potential. In the case of sro in Ni-Mo alloys it was shown that $\langle 1\frac{1}{2}0\rangle$ waves are produced which create imperfectly ordered "average clusters".

Within each domain the degree of order is highest in the middle and decreases toward the edge of the domain according to the composition modulations (see Fig. 12). The width of the domain can vary from three to four {110} $Dl_a$ spacings depending on modulation wavelength resulting from the $S_{lro}/S_{sro}$ ratio. Lattice images in the sro state have shown that the ordered domains contain a maximum of four superlattice planes along $\lambda_{420}$ which is in agreement with the above described model of sro. The weak contrast of the fringes is most probably caused by the small size of the domains, but it may be also due to the low degree of order or to the position of the domains in the foil.[7]

2. <u>Long Range Order in $Au_3Cr$</u>

In the bulk $Au_3Cr$ alloy the $Ll_o$ superlattice has been identified;

a result which has not previously been reported for this alloy. The Dla lro superlattice found in thin films prepared by evaporating $Au_3Cr$[1] most probably arises from loss of chromium during th evaporation process, yielding a composition near $Au_4Cr$. The success of the present investigation was achieved from high quality thin foils, which enabled the weak {100} and {110} superlattice reflections to be detected.

Since the ideal $L1_o$ superlattice corresponds to the AB stoichiometric composition, the formation of this structure can be explained either in terms of microsegregation or a $L1_o$ superstructure containing only 25% of Cr atoms (i.e. nonstoichiometric ordering). If microsegregation occured with chromium rich regions having the $L1_o$ structure, the remaining chromium poor regions should have the right composition for Dla ordering. Since this is not observed, the nonstoichiometric ordering model is more probable. The absence of resolvable splitting of fundamental reflections suggest also that there is little or no composition change between the matrix and ordered domains.

The existence of the $L1_o$ ordered structure may also be explained using the spinodal approach to ordering. Figure 13a shows the possible shape of the composition fluctuations with wavelength equal to the $\underset{\sim}{a}$ parameter and amplitude 0-50% solute. The atomic arrangement in ordered domains is assumed to be that of the $L1_o$ structure, with a 50% probability of occupation of the "right sites" by chromium atoms. The appearance of $\{\frac{1}{2}00\}$ superlattice spots can be explained in a similar way, i.e. they are due to the formation of the transitional ordered phase, which may be represented in terms of modulations along the [100] direction (Fig. 13b), with periodicity equal to the c parameter of the $DO_{22}$ structure. Assuming that the sro is represented by imperfectly ordered $DO_{22}$ microdomains, the change of the position of the (1/2,1/2,

1/2) chromium atom to a random one in the (001) plane leads to the formation of microdomains having the structure described above. This kind of modulation is not stable and is succeeded by modulations of smaller wavelength with amplitude change such that chromium atoms are distributed on every (001) plane. This corresponds to the $L1_o$ structure (fig. 13a).

Nonstoichiometric ordering has also been observed in Cu-29 at %Pt alloy, by Iveronova et al.[13] They explained their results in terms of microsegregation, leading to ordered domains. Such an explanation of nonstoichiometric ordering should, however, be supported by evidence of differences in lattice parameter between the matrix and ordered domains enriched in one of the solute components and from region to region in the specimen. As can be seen from Fig. 2 in the case of formation of the stoichiometric $L1_o$ structure in gold-chromium alloys this lattice parameter difference would be about 0.2Å and it would be easily detectable using conventional diffraction techniques. Without this evidence the spinodal decomposition model, corresponding to composition modulations giving nonstoichiometric ordering seems to be more probable.

3. Domain Interfaces

The lattice imaging technique has also given information on the geometry of domain interfaces in $Au_4Cr$. At resolution levels close to the atomic scale it is possible to measure directly the mismatch of superlattice planes and determine the nature of translational and rotational APB's (Fig. 6) without requiring conventional contrast experiments.

As was shown in Fig. 5, lattice imaging also gives very useful information concerning chemical composition on the atomic scale. From the intensity and distance of the superlattice fringes one can obtain information about the ordering stacking sequence and the relative degree of order of the particular plane. Using this technique it was found, for example, that the dissociated antiphase boundary can also be attached to a faulted ordering stacking sequence, while in Ni-Mo alloys,[10] this kind of APB was found to be attached to dislocations, twin tips or translational APBs. Other information, which can be obtained from lattice images is the distribution of ordered atoms very close to the APB, and the measurement of the real width of the domain boundary. Neither of these can be obtained by conventional electron microscopy techniques.

## SUMMARY AND CONCLUSIONS

1. New high resolution studies of sro in $Au_4Cr$ and $Au_3Cr$ alloys have shown the existence of ordered microdomains of size 10-15Å, which is basically in agreement with the composition modulation model of Okamoto and Thomas[2] proposed for Ni-Mo alloys.

2. The transformation from sro into lro in $Au_4Cr$ alloy which occurs during aging below $T_c$ is initiated by the formation of ordered domains showing ordering of chromium atoms on every fifth {531} fcc plane. During further aging the ordering is completed along each fifth {420} and {620} plane, which corresponds to the formation of the Dla superlattice.

3. Lattice imaging has been found to be very useful in the study of the geometry of domain interfaces. Lattice imaging of the $\{\frac{4}{5},\frac{2}{5}0\}$ superlattice planes at close to symmetrical orientation has shown directly the nature of translational, rotational and dissociated anti-phase boundaries. Two types of translational APB, corresponding to the $a\frac{1}{5}$ <420> and $a\frac{2}{5}$ <420> translation of the superlattice planes were observed.

4. Disc shaped domains on {001}, having the $L1_o$ superlattice structure were observed after aging below $T_c$ in the $Au_3Cr$ alloy. Their formation is preceeded by a transitional ordered phase, which can be described in terms of composition modulations along the [001] direction, with wavelength equal to the c parameter of the $DO_{22}$ structure, i.e. 8Å. Since no microsegregation of solute was detected by x-ray and electron diffraction measurements, the nonstoichiometric $L1_o$ superlattice may be represented in terms of composition modulations of chromium atoms of wavelength equal to the a parameter of the fcc lattice and amplitude 0-50% solute.

ACKNOWLEDGEMENTS

This work was supported by the U.S. Energy Research and Development Administration through the Inorganic Materials Research Division, Lawrence Berkeley Laobratory, University of California, Berkeley, California and by the National Academy of Sciences, Washington DC. The authors are grateful to Dr. R. Sinclair for many helpful discussions.

0 0 0 0 4 2 0 7 8 8 8



## REFERENCES


1. L.E. Tanner, P.C. Clapp and R.S. Toth, Mat. Res. Bull. 3, 855 (1968).
2. P.R. Okamoto and G. Thomas, Acta. Met., 19, 825 (1971).
3. S.K. Das, P.R. Okamoto, P.M.J. Fisher and G. Thomas, Acta. Met., 21, 913 (1973).
4. S.K. Das and G. Thomas, Order-Disorder Transformations in Alloys, p. 332, Edited by H. Warlimont, Springer Verlag (1974).
5. H.E. Cook, D. de Fontaine and J.E. Hilliard, Acta. Met., 17, 765 (1969). Also D. de Fontaine, Acta Met in press (UCLA report 34P201-11 1974).
6. J.M. Cowley, Proceedings of 30th Annual EMSA Meeting, p. 560, Ed. C.J. Arceneaux, Claitor's Publishing Division, Baton Rouge, LA (1972).
7. R. Sinclair, K. Schneider and G. Thomas, Acta Met. (in press), LBL Report 3194.
8. S. Iijima and J.G. Allpress, Acta Cryst., A30, 30 (1974).
9. A. Rocher, J. Dutkiewicz and G. Thomas, to be published.
10. S. Amelinckx, J. Less-common Metals, 28, 325 (1972).
11. S. Iijima, S. Kimura and M. Goto, Acta. Cryst., A30, 251 (1974).
12. L.E. Tanner, Phys. Stat., Sol., 30,685 (1968).
13. V.I. Iveronova, A.A. Katsnelson, Order-Disorder Transformations in Alloys, p. 306, Ed. H. Warlimont, Springer-Verlag (1974).

## FIGURE CAPTIONS

FIG. 1. The schematic representation of atomic arrangement in D1a, $DO_{22}$ and $L1_o$ ordered structures existing in ordered $Au_4Cr$ and $Au_3Cr$ alloys.

FIG. 2. The relationship between the fcc $a_o$ lattice parameter measured using x-ray diffraction in the as-quenched state vs. chromium content.

FIG. 3. Evaporated thin film of $Au_4Cr$ (a) [001] diffraction pattern after quenching from 400°C (b) $\{\frac{1}{2}00\}$ superlattice dark field micrograph (c) [001] orientation after aging for 16 h at 270°C (d) $\{1\frac{3}{5},\frac{1}{5}\}$ superlattice dark field micrograph after tilting around the $[1\bar{1}0]$ axis, with orientation close to $[11\bar{8}]$ (e) [001] orientation after aging for 70 h at 270°C (f) $\{\frac{4}{5},\frac{2}{5}0\}$ superlattice dark field micrograph.

FIG. 4. The lattice image taken from $Au_4Cr$ after quenching from 400°C; A shows $(\frac{1}{2}10)$ 3.6Å fringes, B the cross grating of the lattice fringes from the two variants of microdomains. The position of the objective aperture is marked on the diffraction pattern shown in the corner of the micrograph.

FIG. 5. Lattice image taken from partially ordered $Au_4Cr$ aged for 16 h at 270°C showing the $\{\frac{1}{5},\frac{3}{5}1\}$ of spacing 3.4Å, $\{\frac{4}{5},\frac{2}{5}0\}$ of spacing 4.5Å and 7.0Å Moiré fringes. In A, arrows indicate the faulted ordering stacking sequence which dissociates into two translational APB's. In B, the faulted ordering stacking sequence changes its orientation to become a translational APB.

FIG. 6. The lattice image taken from fully ordered $Au_4Cr$ alloy aged for 70h at 270°C showing the two variants of the 4.5Å $\{\frac{4}{5},\frac{2}{5}0\}$ fringes. A and B indicate two types of translational APB's, corresponding to the translation vector $a\frac{2}{5}$ <420> and $a\frac{1}{5}$ <420> respectively.

FIG. 7. Scheme, illustrating the atomic arrangement in the area marked by a square in Fig. 6.

FIG. 8. Electrolytically thinned foil of $Au_3Cr$ (a) [001] diffraction pattern after quenching from 400°C (b) $(\frac{1}{2}00)$ superlattice dark field micrograph (c) [001] orientation after aging 5 days at 270°C (d) $(1\frac{1}{2}0)$ superlattice dark field micrograph (e) (100) superlattice dark field micrograph (f) [001] orientation after aging 30 days at 300°C (g) $(1\frac{1}{2}0)$ superlattice dark field micrograph (h) (100) superlattice dark field micrograph. For convenience of display the SAD's are not rotated with respect to the images.

FIG. 9. Thin foil of $Au_3Cr$ (a) [001] diffraction pattern after quenching from 400°C (b) bright field (c) (010) superlattice dark field micrograph (d) (110) superlattice dark field micrograph (e) (100) superlattice dark field micrograph. For convenience of display the SAD is not rotated with respect to the images.

FIG. 10. The lattice image from the thin foil of $Au_3Cr$ aged for 30 days at 300°C taken at symmetrical orientation. The 4.0Å (100) and 8Å $(\frac{1}{2}00)$ superlattice fringes are seen.

FIG. 11. A comparison of the lattice image taken with tilted illumination and (100) superlattice dark field of partially ordered $Au_3Cr$. Bright regions in the dark field micrograph correlate well with ordered domains visible in the lattice image. Only one domain marked "x" does not appear in the dark field micrograph. (See text).

FIG. 12. A schematic representation of sro state in $Ni_4Mo$ in terms of composition waves, requiring two lro parameters, after Okamoto and Thomas.[2]

FIG. 13. A concentration wave description of (a) nonstoichiometric $L1_o$ lro in $Au_3Cr$ (b) transitional ordered phase appearing in $Au_3Cr$ of wavelength equal to the $DO_{22}$ c parameter, i.e. 8Å.

0 0 0 0 4 2 0 7 8 9 0



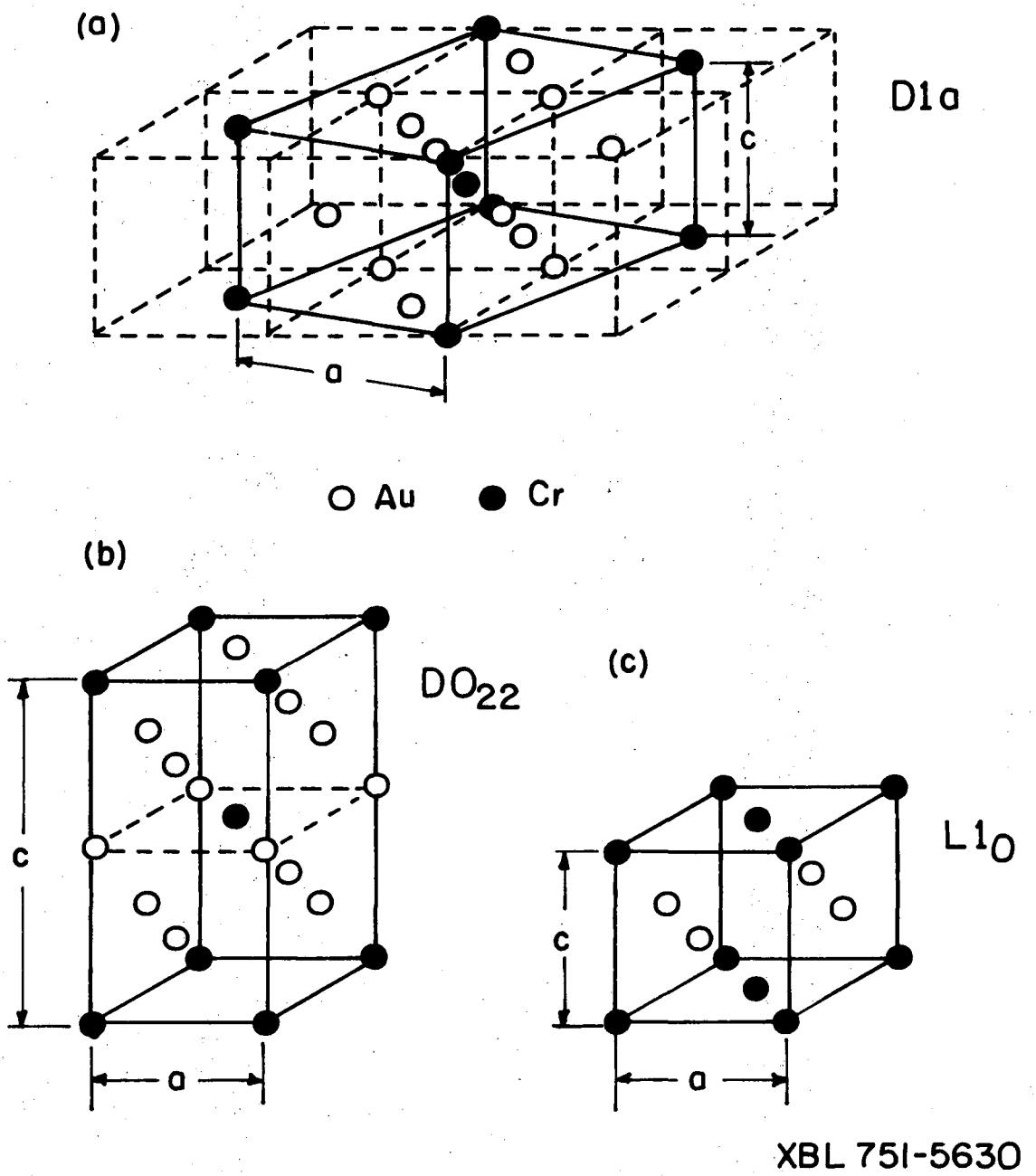


Fig. 1.

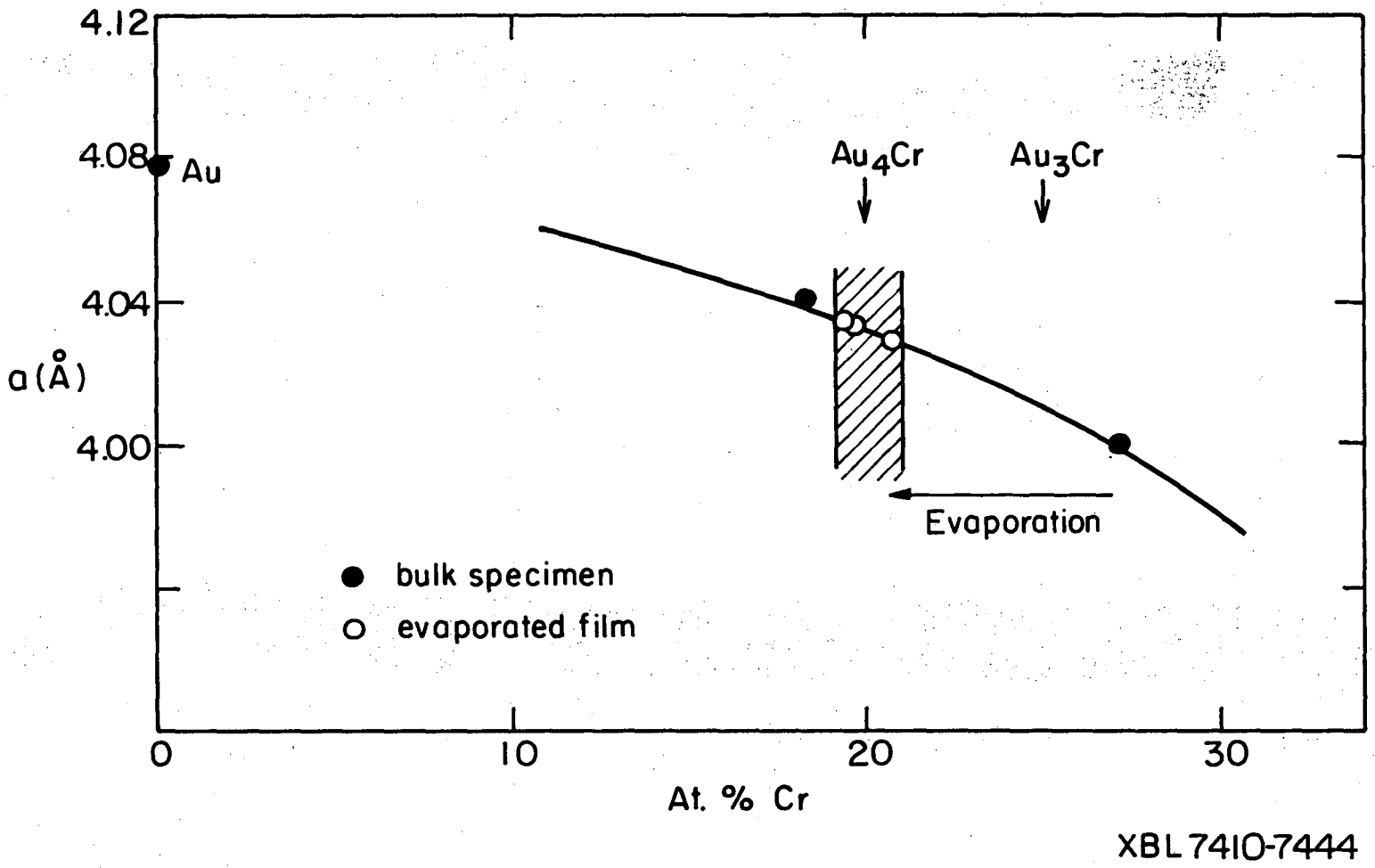
4.12
4.08
4.04
4.00
a (Å)
Au
$Au_4Cr$
$Au_3Cr$
Evaporation
bulk specimen
evaporated film
0
10
20
30
At. % Cr
XBL 7410-7444

Fig. 2.

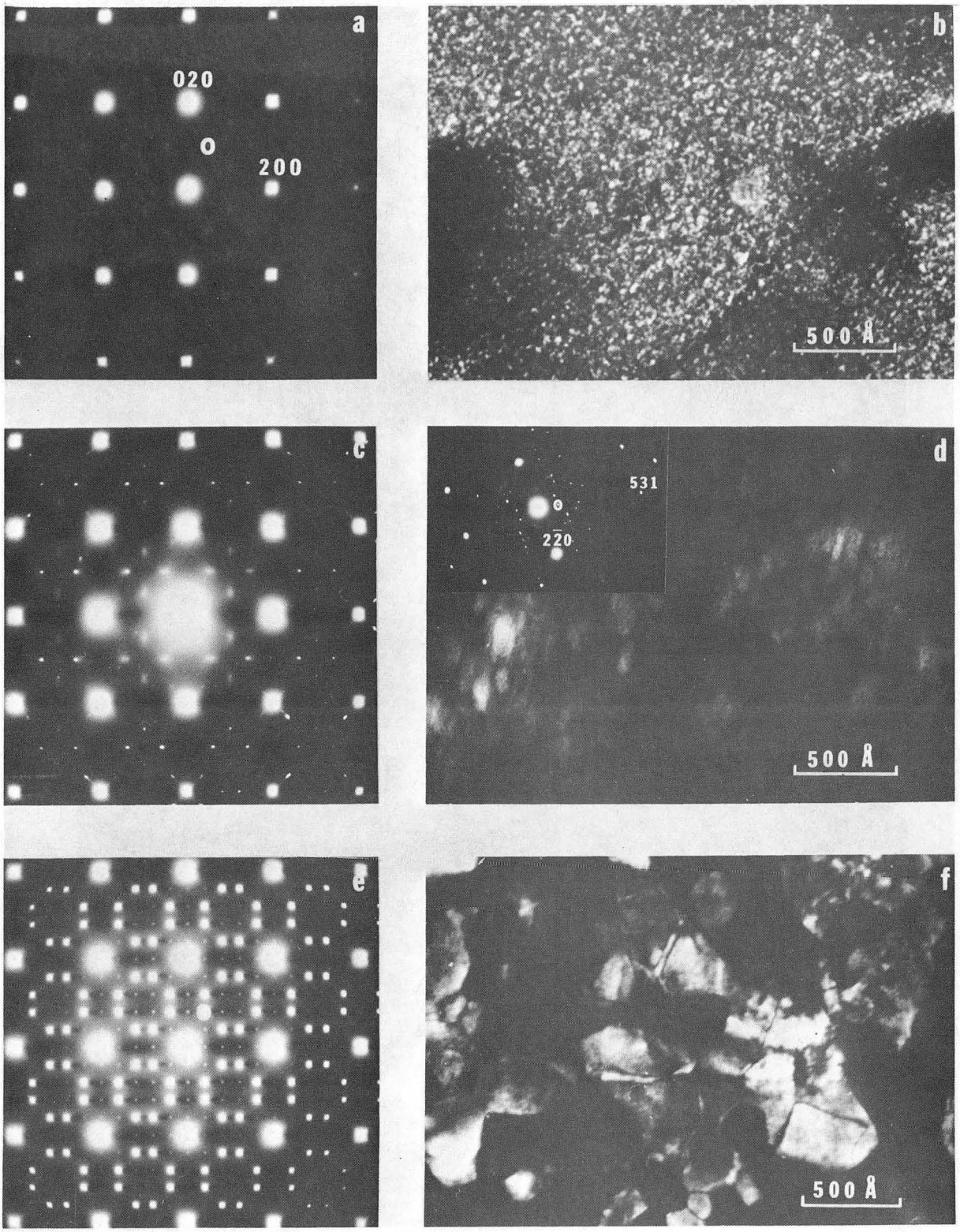


XBB 7410-7330

Fig. 3.

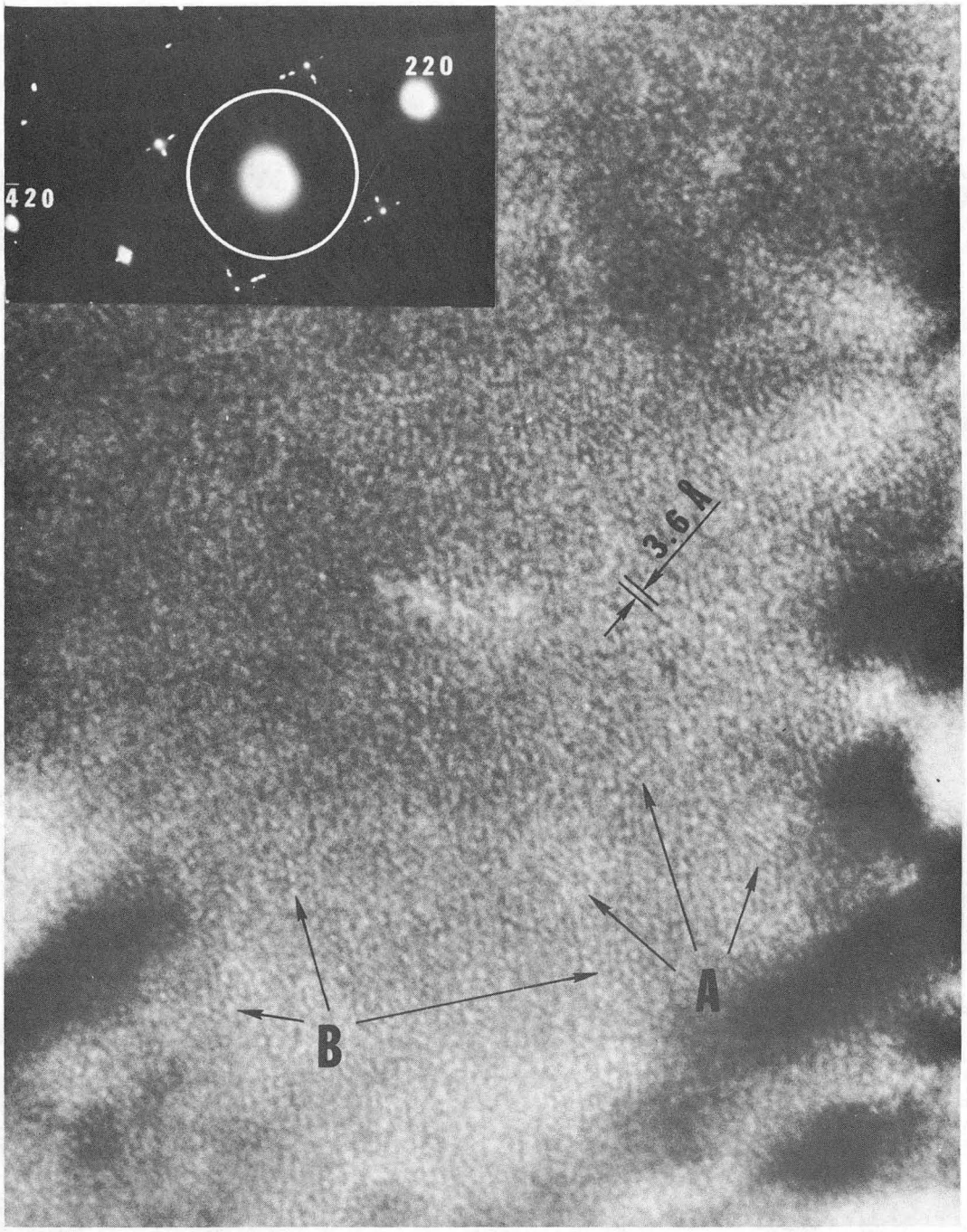


XBB 7410-7327

Fig. 4.

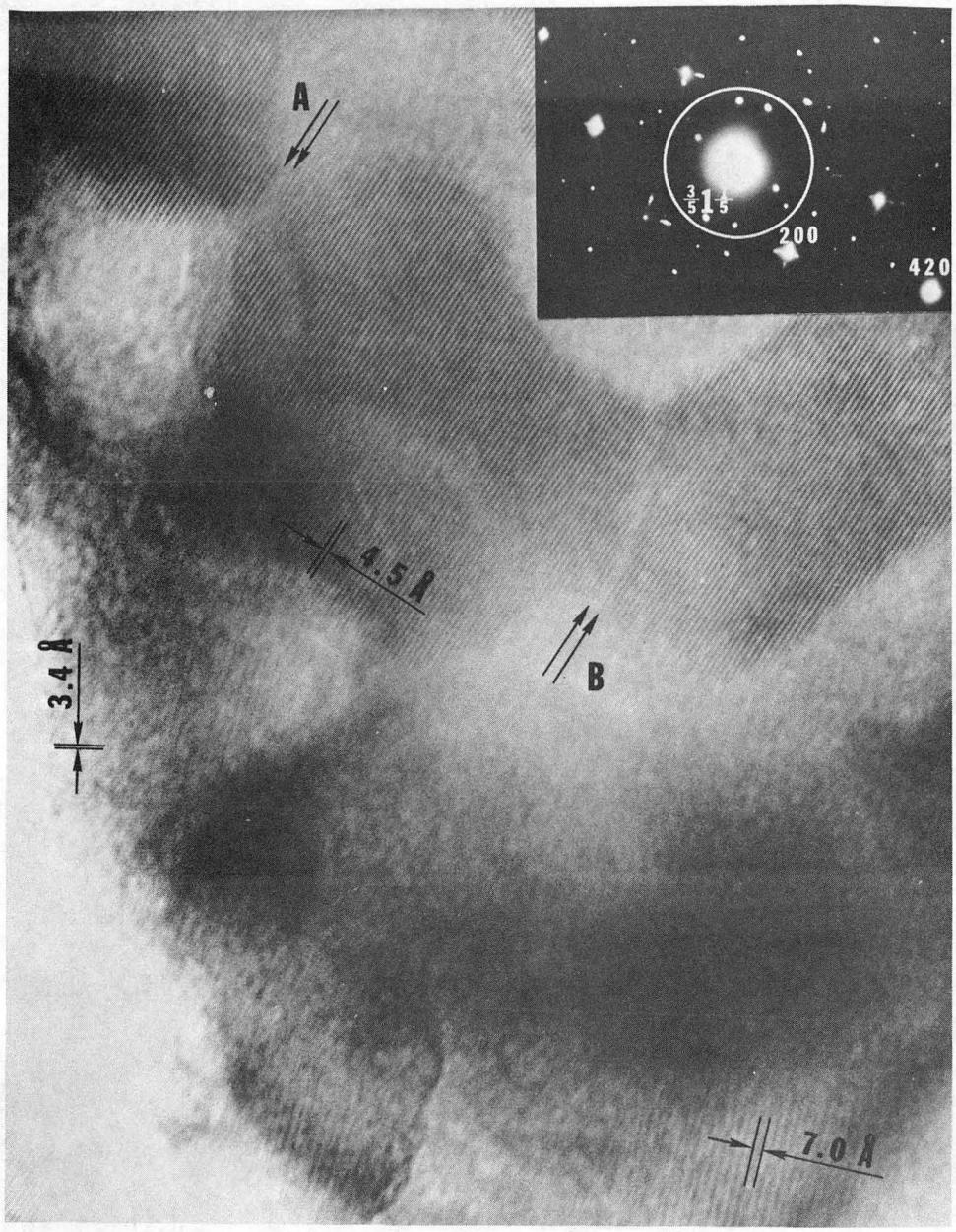


XBB 751-787

Fig. 5.

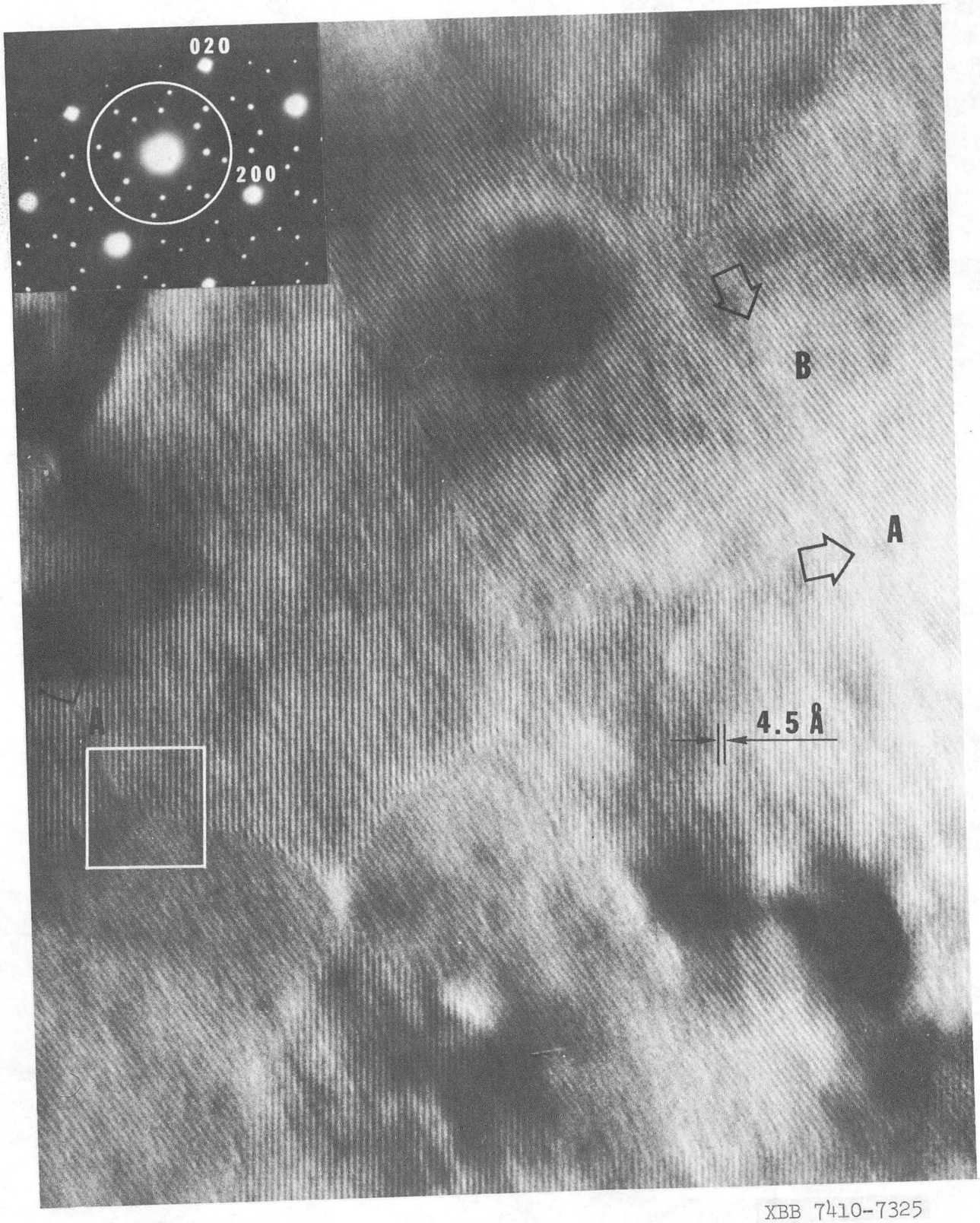


XBB 7410-7325

Fig. 6.

0 0 0 0 4 2 0 7 8 9 3



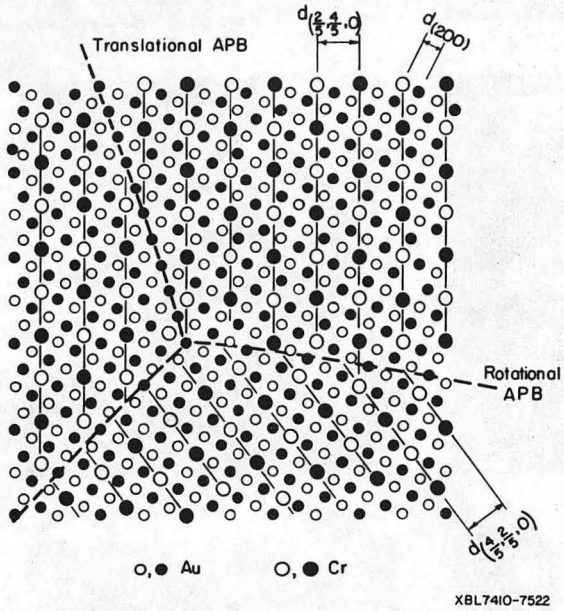


Fig. 7.

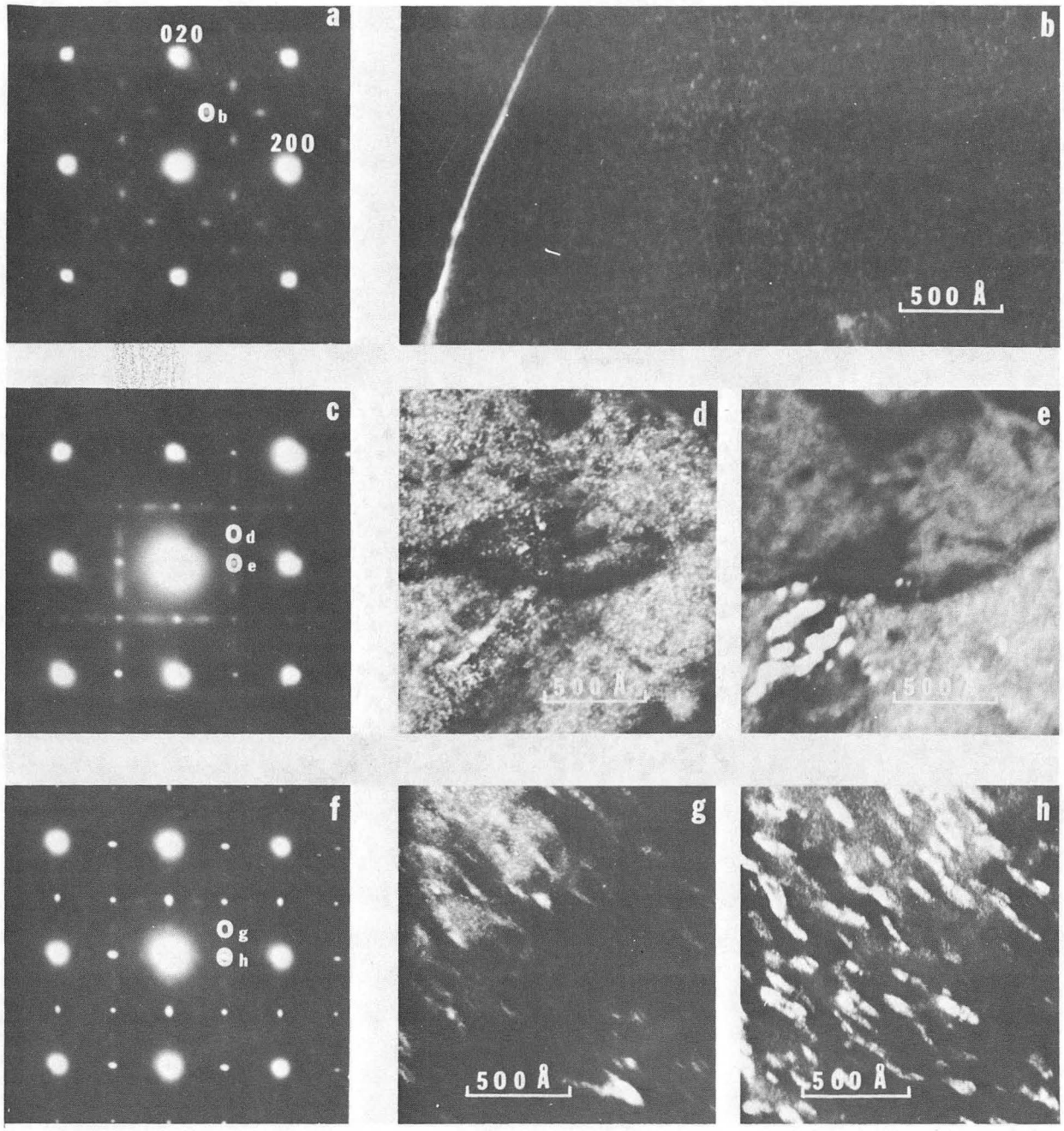


XBB 7410-7329

Fig. 8.

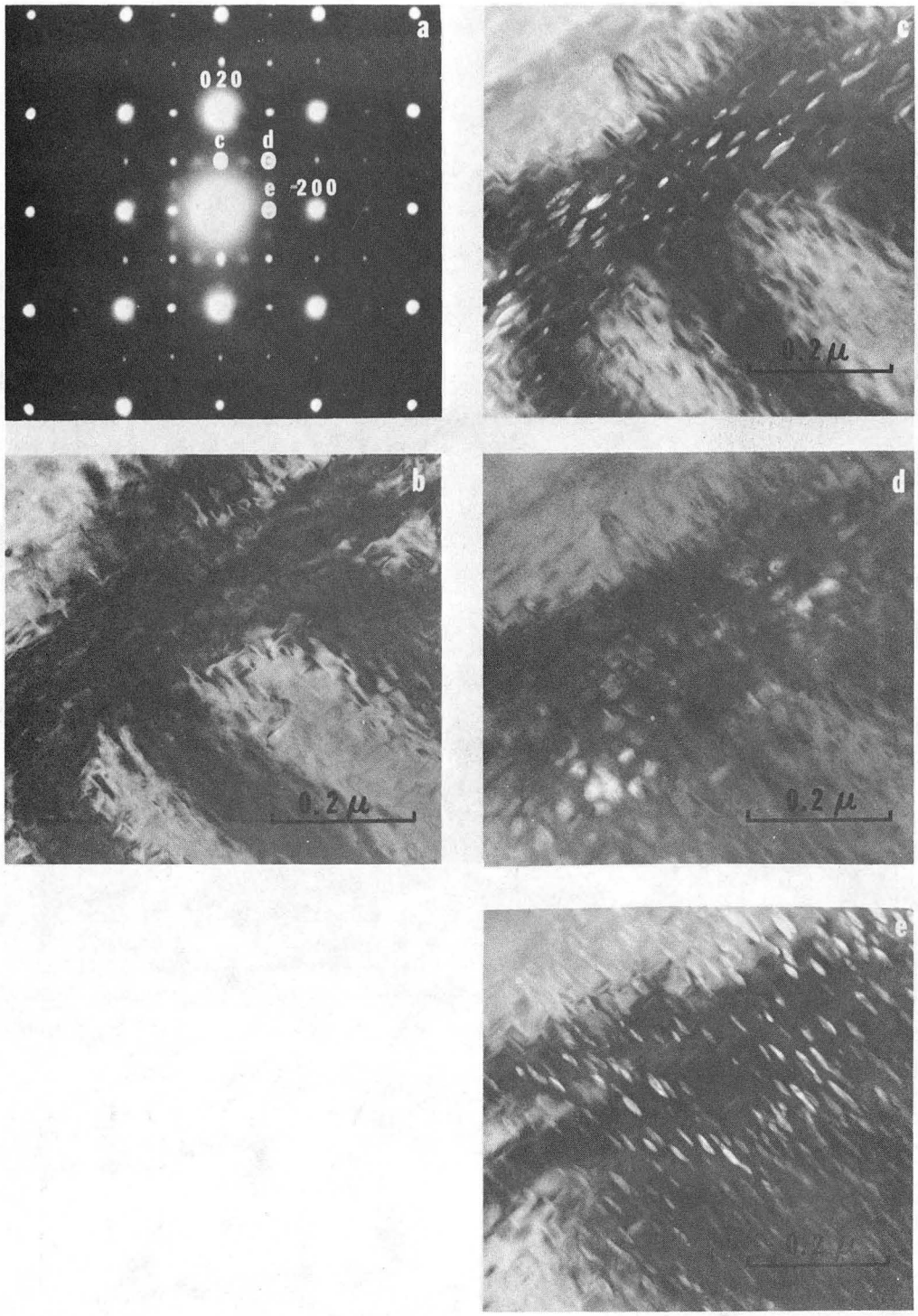


XBB 751-786

Fig. 9.

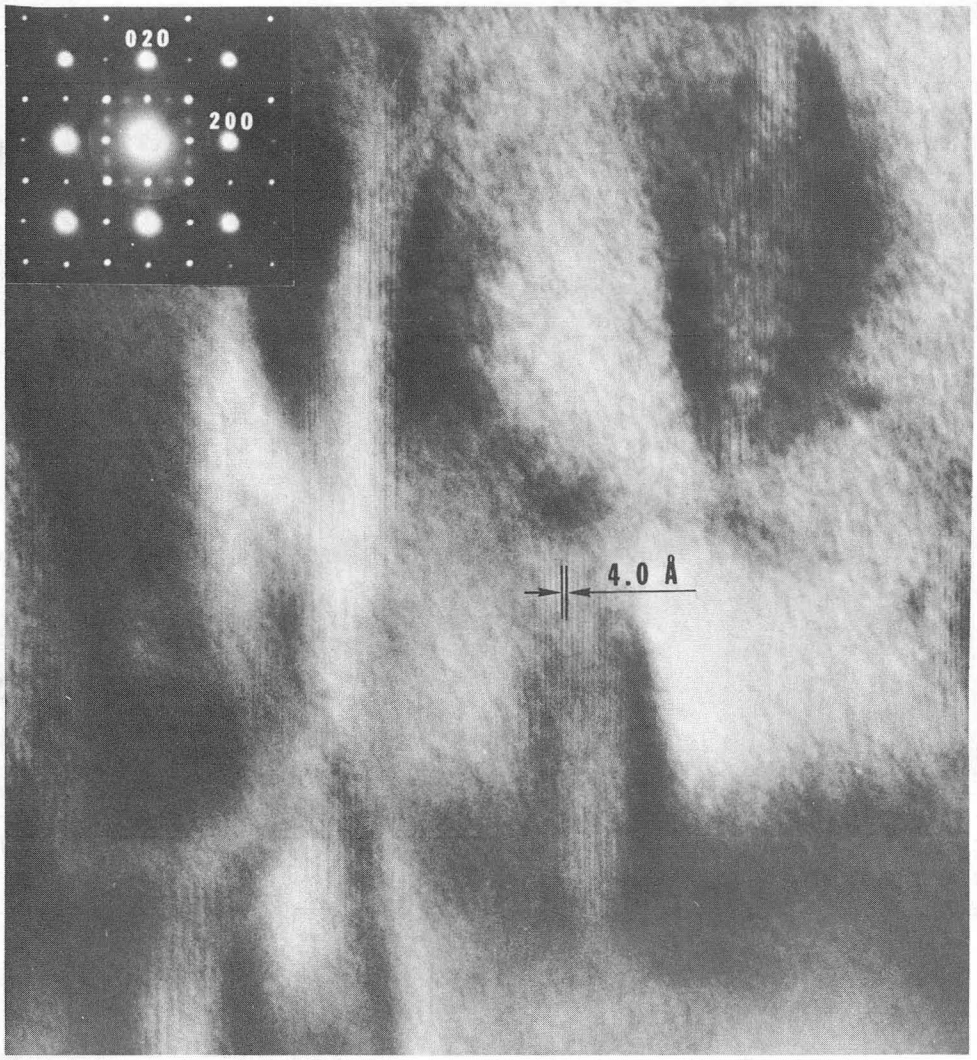


XBB 751-789

Fig. 10.

0 0 0 0 4 2 0 7 8 9 5



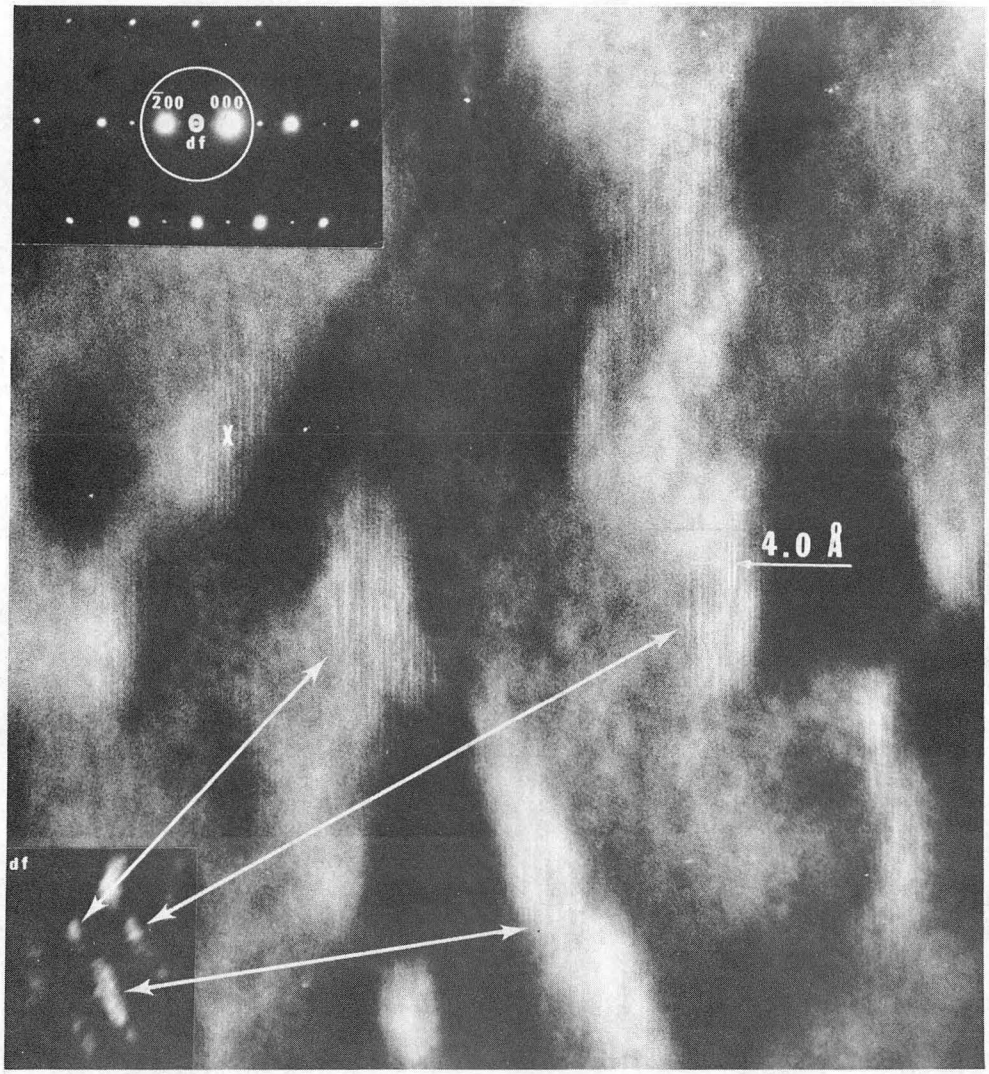


XBB 751-788

Fig. 11.

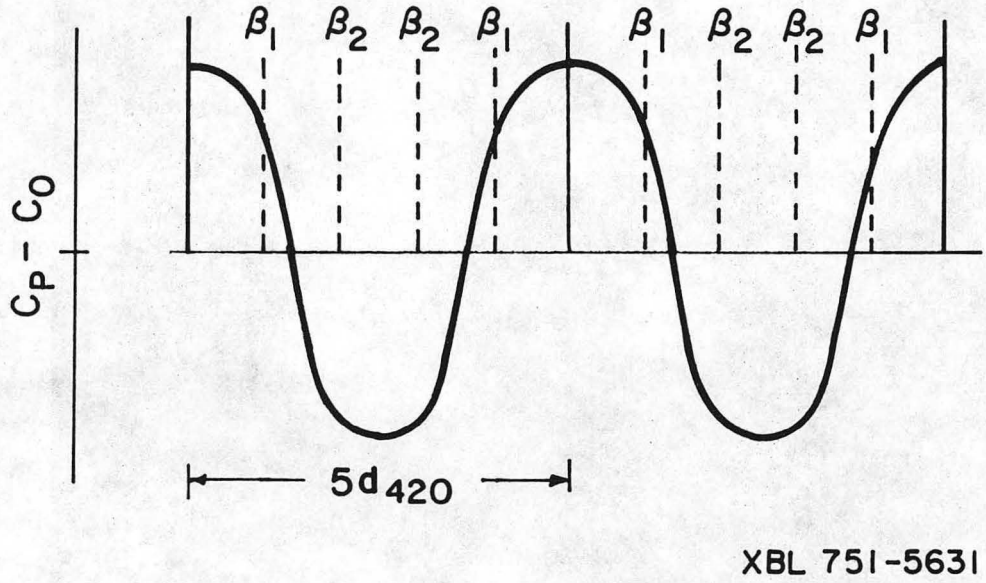


Fig. 12.

0 0 0 0 4 2 0 7 8 9 9 6

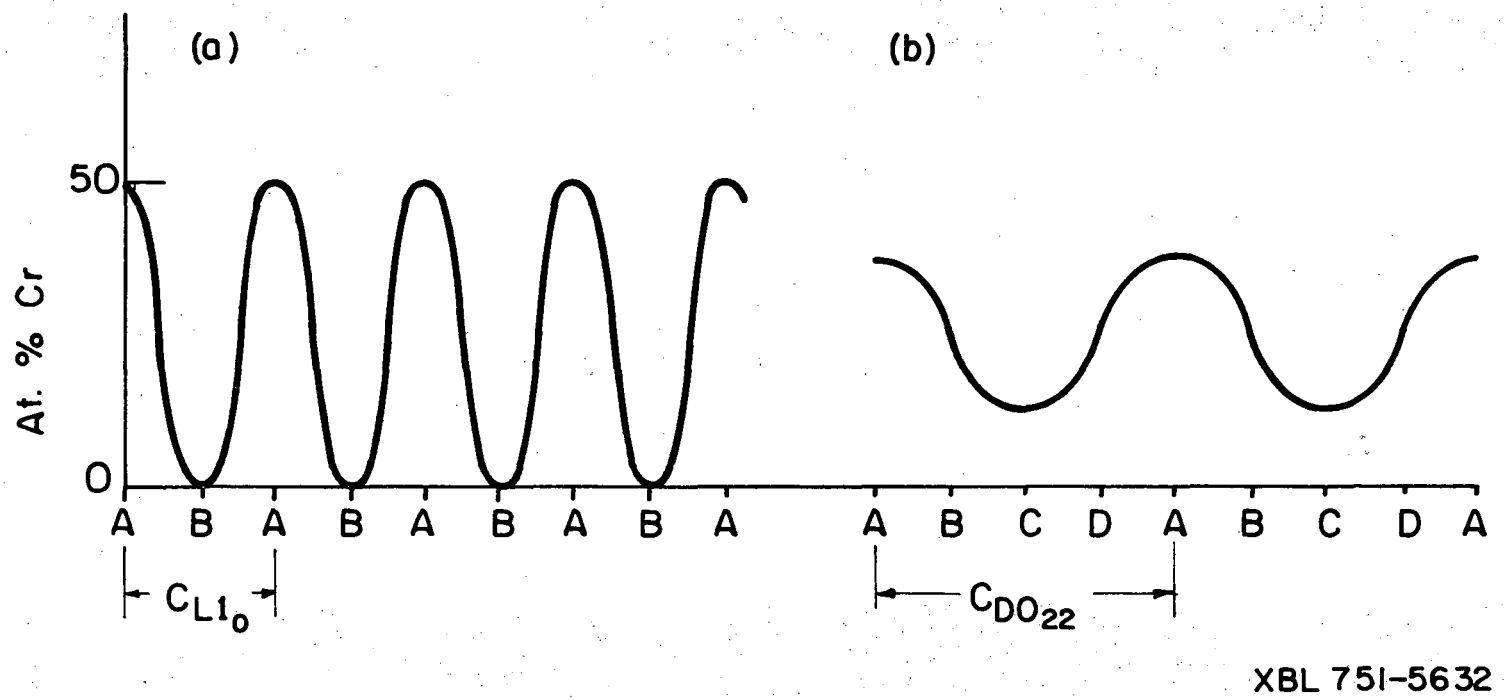


Fig. 13.

0 0 0 0 4 2 0 7 8 9 7

LEGAL NOTICE

*This report was prepared as an account of work sponsored by the United States Government. Neither the United States nor the United States Energy Research and Development Administration, nor any of their employees, nor any of their contractors, subcontractors, or their employees, makes any warranty, express or implied, or assumes any legal liability or responsibility for the accuracy, completeness or usefulness of any information, apparatus, product or process disclosed, or represents that its use would not infringe privately owned rights.*

*TECHNICAL INFORMATION DIVISION*
*LAWRENCE BERKELEY LABORATORY*
*UNIVERSITY OF CALIFORNIA*
*BERKELEY, CALIFORNIA 94720*